

Critical current destabilizing perpendicular magnetization by the spin Hall effect

Tomohiro Taniguchi¹, Seiji Mitani², and Masamitsu Hayashi²

¹*National Institute of Advanced Industrial Science and Technology (AIST),
Spintronics Research Center, Tsukuba 305-8568, Japan*

²*National Institute for Materials Science, Tsukuba 305-0047, Japan*

(Dated: July 5, 2018)

The critical current needed to destabilize the magnetization of a perpendicular ferromagnet via the spin Hall effect is studied. Both the dampinglike and fieldlike torques associated with the spin current generated by the spin Hall effect is included in the Landau-Lifshitz-Gilbert equation to model the system. In the absence of the fieldlike torque, the critical current is independent of the damping constant and is much larger than that of conventional spin torque switching of collinear magnetic systems, as in magnetic tunnel junctions. With the fieldlike torque included, we find that the critical current scales with the damping constant as α^0 (i.e., damping independent), α , and $\alpha^{1/2}$ depending on the sign of the fieldlike torque and other parameters such as the external field. Numerical and analytical results show that the critical current can be significantly reduced when the fieldlike torque possesses the appropriate sign, i.e. when the effective field associated with the fieldlike torque is pointing opposite to the spin direction of the incoming electrons. These results provide a pathway to reducing the current needed to switch magnetization using the spin Hall effect.

PACS numbers: 75.78.-n, 75.70.Tj, 75.76.+j, 75.40.Mg

I. INTRODUCTION

The spin Hall effect¹⁻³ (SHE) in a nonmagnetic heavy metal generates pure spin current flowing along the direction perpendicular to an electric current. The spin current excites magnetization dynamics in a ferromagnet attached to the nonmagnetic heavy metal by the spin-transfer effect^{4,5}. There have been a number of experimental reports on magnetization switching and steady precession induced by the spin Hall effect⁶⁻⁹. These dynamics have attracted great attention recently from the viewpoints of both fundamental physics and practical applications.

An important issue to be solved on the magnetization dynamics triggered by the spin Hall effect is the reduction of the critical current density needed to destabilize the magnetization from its equilibrium direction, which determines the current needed to switch the magnetization direction or to induce magnetization oscillation. The reported critical current density for switching^{8,10-13} or precession⁹ is relatively high, typically larger than 10^7 A/cm². One of the reasons behind this may be related to the recently predicted damping constant independent critical current when SHE is used^{14,15}. This is in contrast to spin-transfer-induced magnetization switching in a typical giant magnetoresistance (GMR) or magnetic tunnel junction (MTJ) device where the critical current is expected to be proportional to the Gilbert damping constant α . Here the magnetization dynamics is excited as a result of the competition between the spin torque and the damping torque¹⁶. Since the damping constant for typical ferromagnet in GMR or MTJ devices is relatively small ($\alpha \sim 10^{-2} - 10^{-3}$)^{17,18}, it can explain why the critical current is larger for the SHE driven systems. Thus in particular for device application purposes, it is crucial to find experimental conditions in which the mag-

netization dynamics can be excited with lower current.

Another factor that might contribute to the reduction of the critical current is the presence of the field like torque¹⁹. In the GMR/MTJ systems, both the conventional spin torque, often referred to as the dampinglike torque, and the fieldlike torque arise from the spin transfer between the conduction electrons and the magnetization^{4,19-23}. Due to the short relaxation length of the transverse spin of the conduction electrons^{24,25}, the damping like torque is typically larger than the fieldlike torque. Indeed, the magnitude of the field like torque experimentally found in GMR/MTJ systems has been reported to be much smaller than the damping like torque²⁶⁻²⁹. Because of its smallness, the fieldlike torque had not been considered in estimating the critical current in the GMR/MTJ systems^{16,30-32}, although it does play a key role in particular systems^{33,34}. In contrast, recent experiments found that the fieldlike torque associated with the SHE is larger than the damping like torque³⁵⁻⁴⁰.

The physical origin of the large SHE-induced fieldlike torque still remains unclear. Other possible sources can be the Rashba effect^{36,41-44}, bulk effect⁴⁵, and the out of plane spin orbit torque⁴⁶. Interestingly, the field like torque has been reported to show a large angular dependence^{36,37,47} (the angle between the current and the magnetization), which cannot be explained by the conventional formalism of spin-transfer torque in GMR/MTJ systems. The fieldlike torque acts as a torque due to an external field and modifies the energy landscape of the magnetization. As a result, a large fieldlike torque can significantly influence the critical current. However, the fieldlike torque had not been taken into account in considering the current needed to destabilize the magnetization from its equilibrium direction and thus its role is still unclear.

In this paper, we study the critical current needed to

destabilize a perpendicular ferromagnet by the spin Hall effect. The Landau-Lifshitz-Gilbert (LLG) equation with the dampinglike and fieldlike torques associated with the spin Hall effect is solved both numerically and analytically. We find that the critical current can be significantly reduced when the fieldlike torque possesses the appropriate sign with respect to the dampinglike torque. With the fieldlike torque included, the critical current scales with the damping constant as α^0 (i.e., damping independent), α , and $\alpha^{1/2}$, depending on the sign of the fieldlike torque and other parameters. Analytical formulas of such damping-dependent critical current are derived [Eqs. (19)-(21)], and they show good agreement with the numerical calculations. From these results, we find conditions in which the critical current can be significantly reduced compared to the damping-independent threshold, i.e., systems without the fieldlike torque.

The paper is organized as follows. In Sec. II, we schematically describe the system under consideration. We discuss the definition of the critical current in Sec. III. Section IV summarizes the dependences of the critical current on the direction of the damping constant, the in-plane field, and the fieldlike torque obtained by the numerical simulation. The analytical formulas of the critical current and their comparison to the numerical simulations are discussed in Sec. V. The condition at which damping-dependent critical current occurs is also discussed in this section. The conclusion follows in Sec. VI.

II. SYSTEM DESCRIPTION

The system we consider is schematically shown in Fig. 1, where an electric current flowing along the x -direction injects a spin current into the ferromagnet by the spin Hall effect. The magnetization dynamics in the ferromagnet is described by the LLG equation,

$$\frac{d\mathbf{m}}{dt} = -\gamma\mathbf{m} \times \mathbf{H} + \alpha\mathbf{m} \times \frac{d\mathbf{m}}{dt} - \gamma H_s \mathbf{m} \times (\mathbf{e}_y \times \mathbf{m}) - \gamma\beta H_s \mathbf{m} \times \mathbf{e}_y, \quad (1)$$

where γ and α are the gyromagnetic ratio and the Gilbert damping constant, respectively. We assume that the magnetization of the ferromagnet points along the film normal (i.e., along the z axis), and an external in-plane magnetic field is applied along the x or y axis. The total magnetic field \mathbf{H} is given by

$$\mathbf{H} = H_{\text{appl}}\mathbf{n}_H + H_K m_z \mathbf{e}_z, \quad (2)$$

where H_{appl} is the external field directed along the x or y axis and H_K is the uniaxial anisotropy field along the z axis. \mathbf{n}_H and \mathbf{e}_i are unit vectors that dictate the direction of the uniaxial anisotropy field and the i axis, respectively. Here we call the external field along the x and y directions the longitudinal and transverse fields, respectively. The third and fourth terms on the right-hand side of Eq. (1) are the damping like and fieldlike

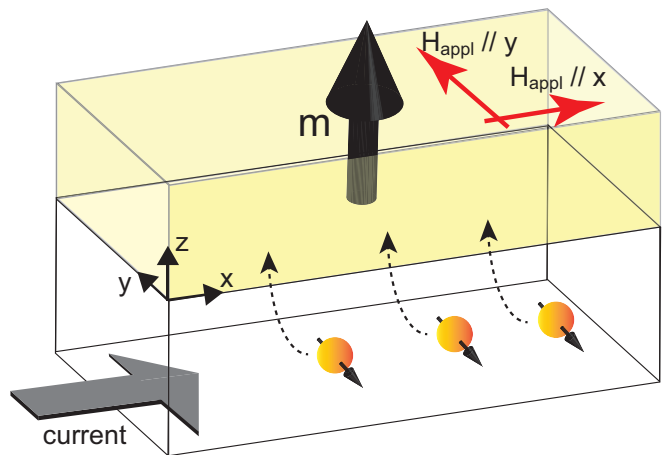


FIG. 1. Schematic view of the spin-Hall system. The x axis is parallel to current, whereas the z axis is normal to the film plane. The spin direction of the electrons entering the magnetic layer via the spin Hall effect points along the $+y$ or $-y$ direction.

torques associated with the spin Hall effect, respectively. The torque strength H_s can be expressed with the current density j , the spin Hall angle ϑ , the saturation magnetization M , and the thickness of the ferromagnet d , i.e.,

$$H_s = \frac{\hbar\vartheta j}{2eMd}. \quad (3)$$

The ratio of the fieldlike torque to the damping like torque is represented by β . Recent experiments found that β is positive and is larger than 1³⁵⁻⁴⁰.

The magnetization dynamics described by the LLG equation can be regarded as a motion of a point particle on a two-dimensional energy landscape. In the presence of the fieldlike torque, the energy map is determined by the energy density given by³⁴

$$\mathcal{E} = -M \int d\mathbf{m} \cdot \mathbf{H} - \beta M H_s \mathbf{m} \cdot \mathbf{e}_y. \quad (4)$$

Then, the external field torque and the fieldlike torque, which are the first and fourth terms on the right-hand-side of Eq. (1), can be expressed as $-\gamma\mathbf{m} \times \mathcal{B}$, where the effective field \mathcal{B} is

$$\mathcal{B} = -\frac{\partial \mathcal{E}}{\partial M \mathbf{m}}. \quad (5)$$

The initial state of the numerical simulation is chosen to be the direction corresponding to the minimum of the effective energy density \mathcal{E} . The explicit forms of the initial state for the longitudinal and the transverse external fields are shown in Appendix A.

We emphasize for the latter discussion in Sec. V that, using Eqs. (1), (4), and (5), the time change of the effective energy density is described as

$$\frac{d\mathcal{E}}{dt} = \frac{d\mathcal{E}_s}{dt} + \frac{d\mathcal{E}_\alpha}{dt}. \quad (6)$$

Here the first and second terms on the right-hand side are the rates of the work done by the spin Hall torque and the dissipation due to damping, respectively, which are explicitly given by

$$\frac{d\mathcal{E}_s}{dt} = \gamma M H_s [\mathbf{e}_y \cdot \mathcal{B} - (\mathbf{m} \cdot \mathbf{e}_y) (\mathbf{m} \cdot \mathcal{B})], \quad (7)$$

$$\frac{d\mathcal{E}_\alpha}{dt} = -\alpha \gamma M [\mathcal{B}^2 - (\mathbf{m} \cdot \mathcal{B})^2]. \quad (8)$$

The sign of Eq. (7) depends on the current direction and the effective magnetic field, while that of Eq. (8) is always negative.

The magnetic parameters used in this paper mimic the conditions achieved in CoFeB/MgO heterostructures⁴⁸; $M = 1500$ emu/c.c., $H_K = 540$ Oe, $\vartheta = 0.1$, $\gamma = 1.76 \times 10^7$ rad/(Oe s), and $d = 1.0$ nm. The value of β is varied from -2 , 0 , to 2 . Note that we have used a reduced H_K (Refs.^{8,49}) in order to obtain critical currents that are the same order of magnitude with that obtained experimentally. We confirmed that the following discussions are applicable for a large value of H_K (~ 1 T).

III. DEFINITION OF CRITICAL CURRENT

In this section, we describe how we determine the critical current from the numerical simulations. In experiments, the critical current is determined from the observation of the magnetization reversal^{8,12,41,46,48-50}. As mentioned in Sec. II, in this paper, the initial state for calculation is chosen to be the minimum of the effective energy density. Usually, there are two minimum points above and below the xy plane because of the symmetry. Throughout this paper, the initial state is chosen to be the minimum point above the xy plane, i.e., $m_z(0) > 0$, for convention.” It should be noted that, once the magnetization arrives at the xy plane during the current application, it can move to the other hemisphere after the current is turned off due to, for example, thermal fluctuation. Therefore, here we define the critical current as the minimum current satisfying the condition

$$\lim_{t \rightarrow \infty} m_z(t) < \epsilon, \quad (9)$$

where a small positive real number ϵ is chosen to be 0.001. The duration of the simulations is fixed to $5 \mu\text{s}$, long enough such that all the transient effects due to the current application are relaxed. Figures 2(a) and 2(b) show examples of the magnetization dynamics close to the critical current, which are obtained from the numerical simulation of Eq. (1). As shown, the magnetization stays near the initial state for $j = 3.1 \times 10^6$ A/cm², while it moves to the xy plane for $j = 3.2 \times 10^6$ A/cm². Thus, the critical current is determined as 3.2×10^6 A/cm² in this case.

We note that the choice of the definition of the critical current has some arbitrariness. For comparison, we

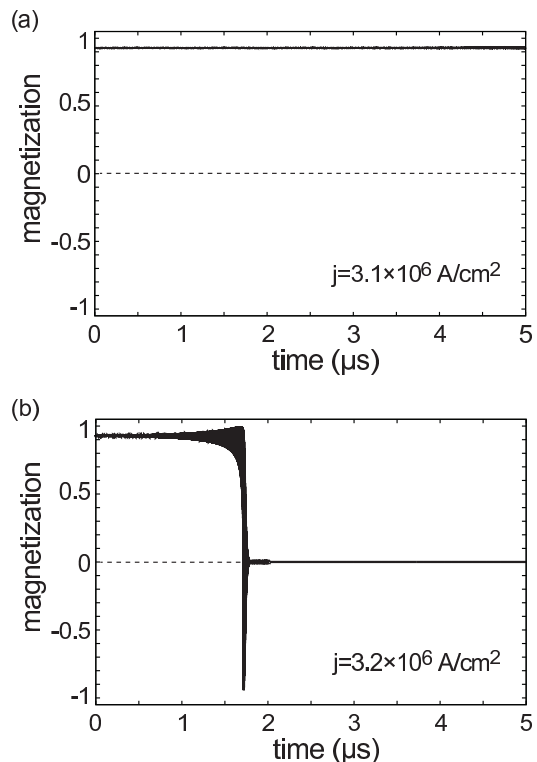


FIG. 2. Time evolution of the z component of the magnetization m_z in the presence of the transverse field of $H_{\text{appl}} = 200$ with (a) $j = 3.1 \times 10^6$ A/cm² and (b) $j = 3.2 \times 10^6$ A/cm². The value of β is zero.

show numerically evaluated critical current with a different definition in Appendix B. The main results of this paper, e.g., the dependence of the critical current on the damping constant, are not affected by the definition.

We also point out that the critical current defined by Eq. (9) focuses on the instability threshold, and does not guarantee a deterministic reversal. For example, in the case of Fig. 2(b), the reversal becomes probabilistic because the magnetization, starting along $+z$, stops its dynamics at the xy plane and can move back to its original direction or rotate to a point along $-z$ resulting in magnetization reversal. Such probabilistic reversal can be measured experimentally using transport measurements^{8,12,41,46,49,50} or by studying nucleation of magnetic domains via magnetic imaging⁴⁸. On the other hand, it has been reported that deterministic reversal can take place when a longitudinal in-plane field is applied alongside the current^{41,49}. It is difficult to determine the critical current analytically for the deterministic switching for all conditions since, as in the case of Fig. 2(b), the magnetization often stops at the xy plane during the current application. This occurs especially in the presence of the transverse magnetic field because all torques become zero at $\mathbf{m} = \pm \mathbf{e}_y$ and the dynamics stops. Here we thus focus on the probabilistic reversal.

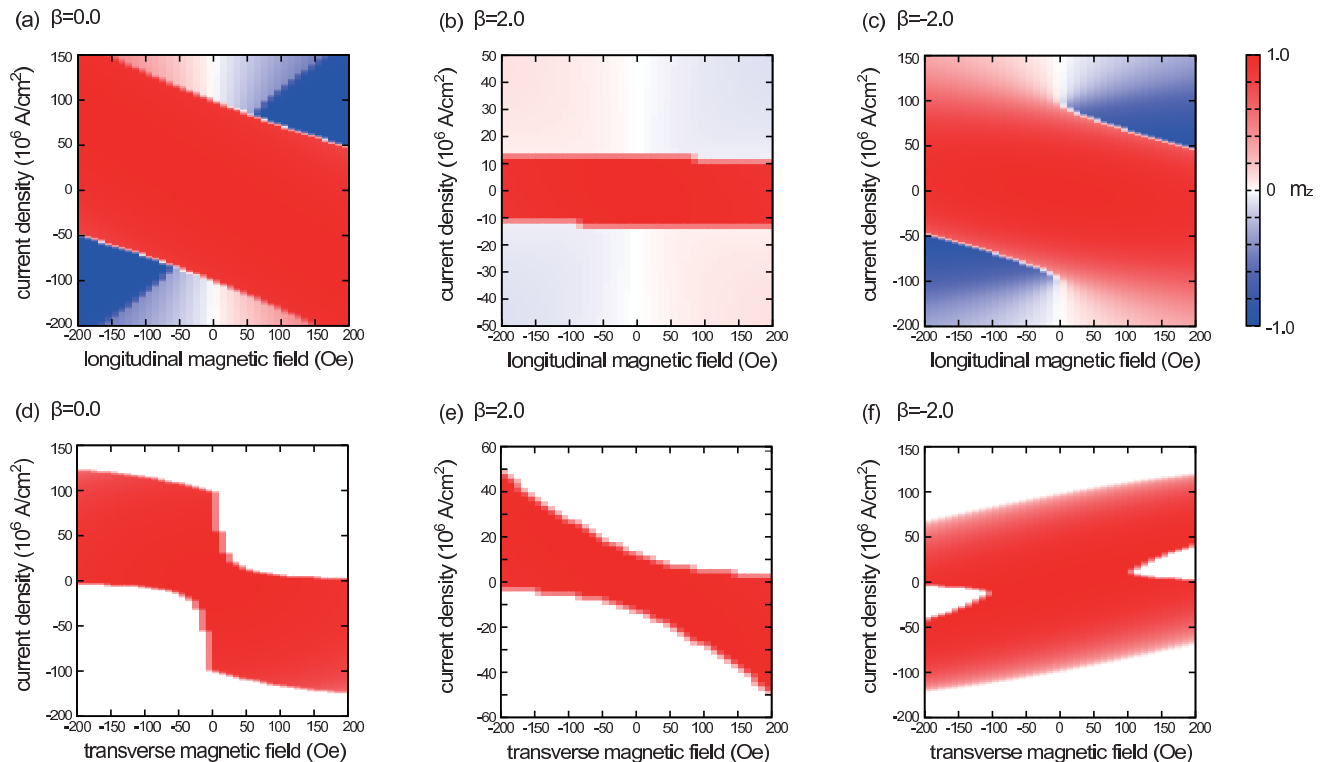


FIG. 3. Numerically evaluated m_z at $t = 5 \mu\text{s}$ for (a)-(c) the longitudinal ($\mathbf{n}_H = \mathbf{e}_x$) and (d)-(f) the transverse ($\mathbf{n}_H = \mathbf{e}_y$) fields, where the value of β is (a), (d) 0.0; (b), (e) 2.0; and (c), (f) -2.0 . The damping constant is $\alpha = 0.005$. The color scale indicates the z component of the magnetization (m_z) at $t = 5 \mu\text{s}$. The red/white boundary indicates the critical current for probabilistic switching, whereas the red/blue boundary gives the critical current for deterministic switching.

IV. NUMERICALLY ESTIMATED CRITICAL CURRENT

In this section, we show numerically evaluated critical current for different conditions. We solve Eq. (1) and apply Eq. (9) to determine the critical current. Figure 3 shows the value of m_z at $t = 5 \mu\text{s}$ in the presence of (a)-(c) the longitudinal ($\mathbf{n}_H = \mathbf{e}_x$) and (d)-(f) the transverse ($\mathbf{n}_H = \mathbf{e}_y$) fields. The value of β is 0 for Figs. 3(a) and 3(d), 2.0 for Figs. 3(b) and 3(e), and -2.0 for Figs. 3(c) and 3(f), respectively. The damping constant is $\alpha = 0.005$. The red/white boundary indicates the critical current for the probabilistic switching, whereas the red and blue ($m_z = -1$) boundary gives the critical current for the deterministic switching. Using these results and the definition of the critical current given by Eq. (9), and performing similar calculations for different values of α , we summarize the dependence of the critical current on the longitudinal and transverse magnetic fields in Fig. 4. The damping constant is varied as the following in each plot: $\alpha = 0.005, 0.01$, and 0.02 . The solid lines in Fig. 4 represent the analytical formula derived in Sec. V.

A. In the presence of longitudinal field

In the case of the longitudinal field and $\beta = 0$ shown in Fig. 4(a), the critical current is damping-independent. Such damping-independent critical current has been reported previously for deterministic magnetization switching^{14,15}. Similarly, in the case of the longitudinal field and negative β ($\beta = -2.0$) shown in Fig. 4(c), the critical current is damping-independent. In these cases, the magnitude of the critical current is relatively high. In particular, near zero field, the critical current exceeds $\sim 10^8 \text{ A/cm}^2$, which is close to the limit of experimentally accessible value. These results indicate that the use of the longitudinal field with zero or negative β is ineffective for the reduction of the critical current.

On the other hand, when β is positive, the critical current depends on the damping constant, as shown in Fig. 4(b). Note that positive β is reported for the torques associated with the spin Hall effect or Rashba effect in the heterostructures studied experimentally^{35-37,39}. The magnitude of the critical current, $\sim 10 \times 10^6 \text{ A/cm}^2$, is relatively small compared with the cases of zero or negative β . In this case, the use of a low damping material is effective to reduce the critical current. Interestingly, the critical current is not proportional to the damping constant, while that previously calculated for a GMR or MTJ system¹⁶ is proportional to α . For example, the

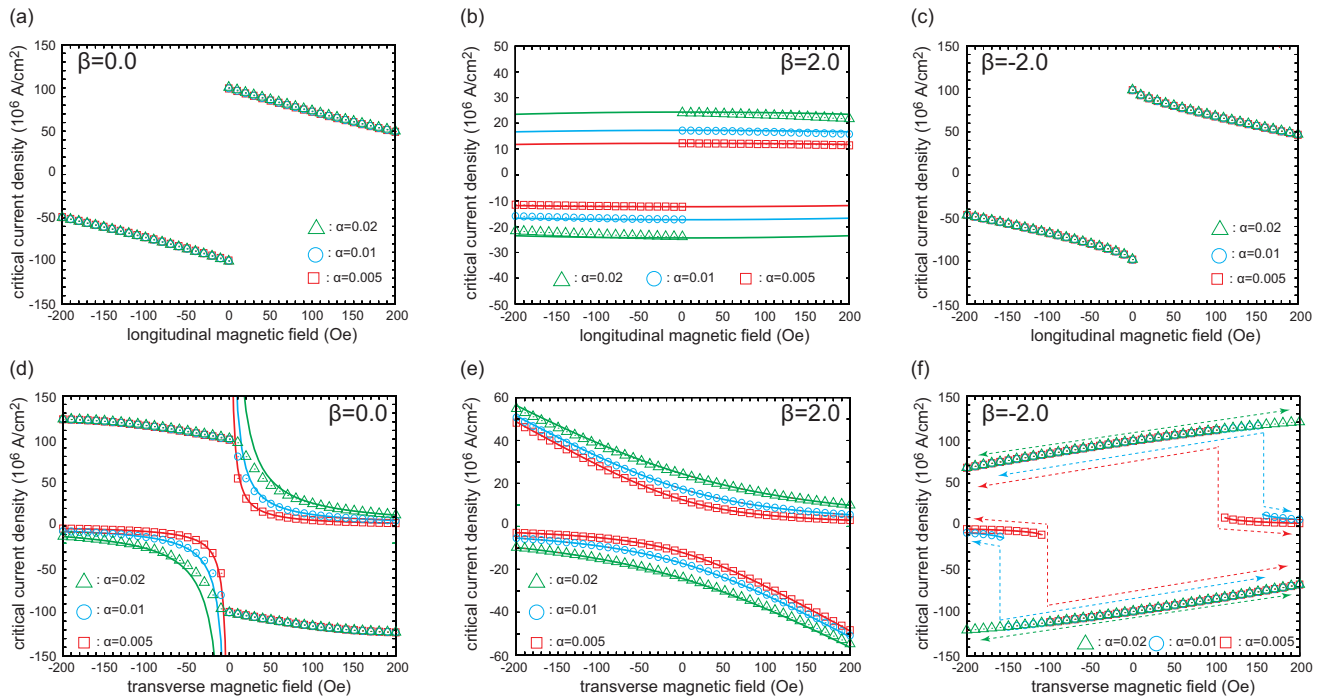


FIG. 4. Numerically evaluated critical currents in the presence of (a)-(c) the longitudinal ($\mathbf{n}_H = \mathbf{e}_x$) and (d)-(f) the transverse ($\mathbf{n}_H = \mathbf{e}_y$) fields, where the value of β is (a), (d) 0.0; (b), (e) 2.0; and (c), (f) -2.0 , respectively. The solid lines are analytically estimated critical current in Sec. V.

critical current at zero longitudinal field in Fig. 4(b) is 12.3 , 17.2 , and 24.0×10^6 A/cm 2 for $\alpha = 0.005$, 0.01 , and 0.02 , respectively. These values indicate that the critical current is proportional to $\alpha^{1/2}$. In fact, the analytical formula derived in Sec. V shows that the critical current is proportional to $\alpha^{1/2}$ for positive β [see Eq. (19)].

To summarize the case of the longitudinal field, the use of a heterostructure with positive β , which is found experimentally, has the possibility to reduce the critical current if a ferromagnet with low damping constant is used. In this case, the critical current is proportional to $\alpha^{1/2}$, which has not been found in previous works.

B. In the presence of transverse field

In the presence of the transverse field with $\beta = 0$, the critical current shows a complex dependence on the damping constant α , as shown in Fig. 4(d). When the current and the transverse field are both positive (or negative), the critical current is proportional to the damping constant α except near zero field. The numerically calculated critical current matches well with the analytical result, Eq. (20), shown by the solid lines. In this case, the use of the low damping material results in the reduction of the critical current. On the other hand, when the current and the transverse field possess the opposite sign, the critical current is damping independent. Moreover, in this case, the critical current is of the order of 10^8 A/cm 2 . Thus, it is preferable to use the current and field having the same sign for the reduction of the critical current. It

should be noted that, in our definition, the same sign of current and field corresponds to the case when the direction of incoming electrons' spin (due to the SHE) and the transverse field are opposite to each other. The reason why the critical current becomes damping dependent in this situation will be explained in Sec. V.

When β is positive the critical current depends on the damping constant for the whole range of the transverse field, as shown in Fig. 4(e). The critical current is roughly proportional to $\alpha^{1/2}$, in particular, close to zero field. The solid lines display the analytical formula, Eq. (21), and show good agreement with the numerical calculations. The damping dependence of the critical current becomes complex when the magnitude of the transverse field is increased [see Eq. (21)]. We note that the critical current for the positive β in Fig. 4(e) is smaller than that for $\beta = 0$ in Fig. 4(d) for the whole range of H_{appl} .

On the other hand, when β is negative, the critical current is almost independent of α , especially near zero field. However, when the transverse field is increased, there is a regime where the critical current depends on the damping constant. Such transition of the critical current with the transverse field is also predicted by the analytical solution, Eq. (21).

To summarize the case of the transverse field, the α dependence of the critical current can be categorized into the following: α^0 (damping independent), α , $\alpha^{1/2}$, or other complex behavior. As with the case of the longitudinal field, the use of a heterostructure with positive β allows reduction of the critical current when low damping ferromagnet is used. Overall, the most efficient condition

to reduce the critical current is to use the transverse field with heterostructures that possess low α and positive β . In this case, the critical current is reduced to the order of 10^6 A/cm².

V. ANALYTICAL FORMULA OF CRITICAL CURRENT

In this section, we derive the analytical formula of the critical current from the linearized LLG equation⁵¹. The complex dependences of the critical current on the damping constant α discussed in Sec. IV are well explained by the analytical formula. We also discuss the physical insight obtained from the analytical formulas.

A. Derivation of the critical current

To derive the critical current, we consider the stable condition of the magnetization near its equilibrium. It is convenient to introduce a new coordinate XYZ in which the Z axis is parallel to the equilibrium direction. The rotation from the xyz -coordinate to the XYZ coordinate is performed by the rotation matrix

$$\mathbf{R} = \begin{pmatrix} \cos\theta & 0 & -\sin\theta \\ 0 & 1 & 0 \\ \sin\theta & 0 & \cos\theta \end{pmatrix} \begin{pmatrix} \cos\varphi & \sin\varphi & 0 \\ -\sin\varphi & \cos\varphi & 0 \\ 0 & 0 & 1 \end{pmatrix}, \quad (10)$$

where (θ, φ) are the polar and azimuth angles of the magnetization at equilibrium. The equilibrium magnetization direction under the longitudinal and transverse magnetic field is given by Eqs. (A1) and (A2), respectively. Since we are interested in small excitation of the magnetization around its equilibrium, we assume that the components of the magnetization in the XYZ coordinate satisfy $m_Z \simeq 1$ and $|m_X|, |m_Y| \ll 1$. Then, the LLG equation is linearized as

$$\frac{1}{\gamma} \frac{d}{dt} \begin{pmatrix} m_X \\ m_Y \end{pmatrix} + \mathbf{M} \begin{pmatrix} m_X \\ m_Y \end{pmatrix} = -H_s \begin{pmatrix} \cos\theta \sin\varphi \\ \cos\varphi \end{pmatrix}, \quad (11)$$

where the components of the 2×2 matrix \mathbf{M} are

$$M_{1,1} = \alpha \mathcal{B}_X - H_s \sin\theta \sin\varphi, \quad (12)$$

$$M_{1,2} = \mathcal{B}_Y, \quad (13)$$

$$M_{2,1} = \mathcal{B}_X \quad (14)$$

$$M_{2,2} = \alpha \mathcal{B}_Y - H_s \sin\theta \sin\varphi. \quad (15)$$

Here, \mathcal{B}_X and \mathcal{B}_Y are defined as

$$\mathcal{B}_X = H_{\text{appl}} \sin\theta \cos(\varphi - \varphi_H) + \beta H_s \sin\theta \sin\varphi + H_K \cos 2\theta, \quad (16)$$

$$\mathcal{B}_Y = H_{\text{appl}} \sin\theta \cos(\varphi - \varphi_H) + \beta H_s \sin\theta \sin\varphi + H_K \cos^2\theta, \quad (17)$$

where φ_H represents the direction of the external field within the xy plane: $\varphi_H = 0$ for the longitudinal field and $\pi/2$ for the transverse field.

The solution of Eq. (11) is $m_X, m_Y \propto \exp\{\gamma[\pm i\sqrt{\det[\mathbf{M}] - (\text{Tr}[\mathbf{M}]/2)^2} - \text{Tr}[\mathbf{M}]/2]t\}$, where $\det[\mathbf{M}]$ and $\text{Tr}[\mathbf{M}]$ are the determinant and trace of the matrix \mathbf{M} , respectively. The imaginary part of the exponent determines the oscillation frequency around the Z axis, whereas the real part determines the time evolution of the oscillation amplitude. The critical current is defined as the current at which the real part of the exponent is zero. Then, the condition $\text{Tr}[\mathbf{M}] = 0$ gives

$$\alpha(\mathcal{B}_X + \mathcal{B}_Y) - 2H_s \sin\theta \sin\varphi = 0, \quad (18)$$

For the longitudinal field, Eq. (18) gives

$$j_c^{\text{LONG}} = \pm \frac{2e\sqrt{\alpha}Md}{\hbar\vartheta} \frac{\sqrt{2H_K^2 - H_{\text{appl}}^2}}{\sqrt{\beta(2 + \alpha\beta)}}, \quad (19)$$

indicating that the critical current is roughly proportional to $\alpha^{1/2}$. This formula works for positive β only⁵² if we assume $0 < 2 + \alpha\beta \simeq 2$, which is satisfied for typical ferromagnets. The critical current when the transverse field is applied reads

$$j_c^{\text{TRANS}} = \frac{2\alpha eMd}{\hbar\vartheta(H_{\text{appl}}/H_K)} H_K \left[1 - \frac{1}{2} \left(\frac{H_{\text{appl}}}{H_K} \right)^2 \right], \quad (20)$$

when $\beta = 0$, indicating that the critical current is proportional to α . The critical current for finite β is

$$j_c^{\text{TRANS}} = \frac{2eMd}{\hbar\vartheta} \times \frac{-(1 + \alpha\beta)H_{\text{appl}} \pm \sqrt{H_{\text{appl}}^2 + 2\alpha\beta(2 + \alpha\beta)H_K^2}}{\beta(2 + \alpha\beta)}. \quad (21)$$

Equation (21) works for the whole range of $|H_{\text{appl}}| (< H_K)$ for positive β , while it only works when $|H_{\text{appl}}| > 2\alpha\beta(2 + \alpha\beta)H_K$ for negative β . For example, when $\beta = -2.0$, this condition is satisfied when $|H_{\text{appl}}| > 108$ Oe for $\alpha = 0.005$ and $|H_{\text{appl}}| > 152$ Oe for $\alpha = 0.01$. However the condition is not satisfied for the present range of H_{appl} for $\alpha = 0.02$. The solid lines in Fig. 4(f) show where Equation (21) is applicable. The zero-field limits of Eqs. (19) and (21) become identical,

$$\lim_{H_{\text{appl}} \rightarrow 0} j_c = \pm \frac{2e\sqrt{\alpha}Md}{\hbar\vartheta} \frac{\sqrt{2}H_K}{\sqrt{\beta(2 + \alpha\beta)}}, \quad (22)$$

indicating that the critical current near zero field is proportional to $\alpha^{1/2}$ when $\beta > 0$.

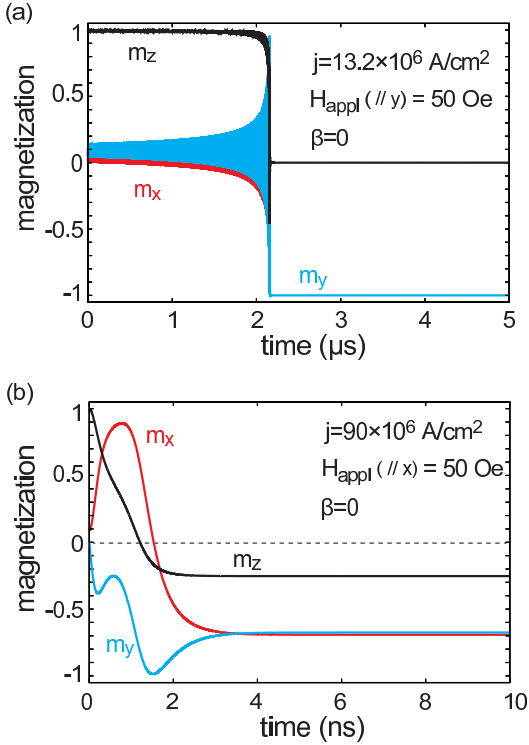


FIG. 5. Magnetization dynamics under the conditions of (a) $\mathbf{n}_H = \mathbf{e}_y$, $H_{\text{appl}} = 50$ Oe, $\beta = 0$, $\alpha = 0.005$, and $j = 13.2 \times 10^6$ A/cm², and (b) $\mathbf{n}_H = \mathbf{e}_x$, $H_{\text{appl}} = 50$ Oe, $\beta = 0$, $\alpha = 0.005$, and $j = 90 \times 10^6$ A/cm².

B. Discussions

The solid lines in Fig. 4(b), 4(d), 4(e), and 4(f) show the analytical formulas, Eqs. (19), (20), and (21). As evident, these formulas agree well with the numerical results in the regions where the critical currents depend on the damping constant. In this section, we discuss the reason why the critical current becomes damping dependent or damping independent depending on the field direction and the sign of β .

It is useful for the following discussion to first study typical magnetization dynamics found in the numerical calculations. Figure 5 shows the time evolution of the x , y and z components of the magnetization when the critical current depends on [Fig. 5(a)] or is independent of [Fig. 5(b)] the damping constant. For the former, the instability is accompanied with a precession of the magnetization. On the other hand, the latter shows that the instability takes place without the precession.

We start with the case when the critical current becomes damping dependent. To provide an intuitive picture, we schematically show in Fig. 6(a) the torques exerted on the magnetization during one precession period when current is applied. The condition is the same with that described in Fig. 5(a), i.e., the transverse magnetic field is applied with $\beta = 0$. In Fig. 6(a), magnetization is shown by the large black arrow, while the directions of the spin Hall torque, the damping torque and the ex-

ternal field torque are represented by the solid, dotted and dashed lines, respectively (the external field torque is tangent to the precession trajectory). As evident in Fig. 5(a), the precession trajectory is tilted to the positive y direction due to the transverse field. Depending on the direction of the magnetization the spin Hall torque has a component parallel, antiparallel, or normal to the damping torque. This means that the work done by the spin Hall torque, denoted by ΔE_s in Fig. 6 (a), is positive, negative, or zero at these positions. This can be confirmed numerically when we calculate the work done by the spin Hall torque using Eq. (7). For an infinitesimal time Δt , the work done by the spin Hall torque is equal to the rate of its work ($d\mathcal{E}_s/dt$), given in Eq. (7), times Δt , i.e. $\Delta E_s = (d\mathcal{E}_s/dt)\Delta t$. The solid line in Fig. 6(b) shows an example of the calculated rate of the work done by the spin Hall torque (solid line), $d\mathcal{E}_s/dt$ in Eq. (7). As shown, $d\mathcal{E}_s/dt$ is positive, negative, and zero, when the magnetization undergoes one precession period. Similarly, the energy dissipated by the damping torque, $d\mathcal{E}_\alpha/dt$, can be calculated using Eq. (8) and is shown by the dotted line in Fig. 6(b). The calculated dissipation due to damping over a precession period is always negative. Details of how the rates, shown in Fig. 6, are calculated are summarized in Appendix C.

Note that the strength of the spin Hall torque for $\Delta E_s > 0$ is larger than that for $\Delta E_s < 0$ due to the angular dependence of the spin Hall torque, $|\mathbf{m} \times (\mathbf{e}_y \times \mathbf{m})|$. Although it is difficult to see, the solid line in Fig. 6(b) is slightly shifted upward. Thus the total energy supplied by the spin Hall torque during one precession, given by $\oint dt(d\mathcal{E}_s/dt)$, does not average to zero and becomes positive. When the current magnitude, $|j|$, is larger than $|j_c|$ in Eq. (20), the energy supplied by the spin Hall torque overcomes the dissipation due to the damping and consequently the precession amplitude grows, which leads to the magnetization instability shown in Fig. 5(a). The same picture is applicable when both directions of field and current are reversed. For this condition, the instability of the magnetization is induced by the competition between the spin Hall torque and the damping torque. Therefore, the critical current depends on the damping constant α . When only the current direction is reversed in Figs. 6(a) and 6(b) (i.e., the sign of the magnetic field and current is opposite to each other), the sign of ΔE_s is reversed and thus the total energy supplied by the spin Hall torque becomes negative. This means that the spin Hall torque cannot overcome the damping torque to induce instability. Therefore, the critical current shown in Eq. (20) only applies to the case when the sign of the field and current is the same. As described in Sec. IV, the same sign of the current and field in our definition means that the incoming electrons' spin direction, due to the spin Hall effect, is opposite to the transverse field direction.

Next, we consider the case when the critical current is damping independent. Figure 6 (c) schematically shows the precession trajectory when the applied field points to

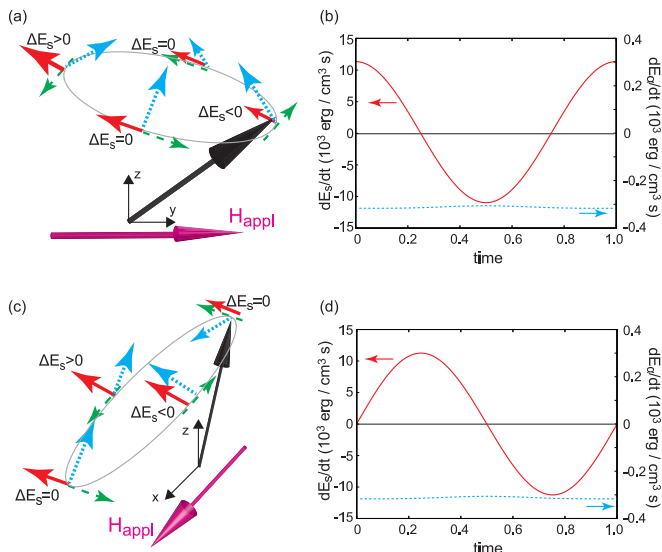


FIG. 6. (a) A schematic view of the precession trajectory in the presence of the applied field in the positive y -direction. The solid and dotted arrows indicate the directions of the spin Hall torque and the damping torque, respectively. The dashed line, which is the tangent line to the precession trajectory, shows the field torque. The damping torque always dissipates energy from the ferromagnet. On the other hand, the spin Hall torque supplies energy ($\Delta E_s > 0$) when its direction is anti-parallel to the damping torque, and dissipates energy ($\Delta E_s < 0$) when the direction is parallel to the damping torque. When the direction of the spin Hall torque is orthogonal to the damping torque, the spin Hall torque does not change the energy ($\Delta E_s = 0$). (b) Typical temporal variation of the rates of the work done by the spin Hall torque, Eq. (7), (solid) and the dissipation due to damping, Eq. (8) (dotted) in the presence of the transverse field. The time is normalized by the period given by Eq. (C7). (c), (d) Similar figures with the longitudinal field.

the x direction and $\beta = 0$. The corresponding rate of work done by the spin Hall torque and the dissipation rate due to the damping torque are shown in Fig. 6 (d). Similar to the previous case, ΔE_s can be positive, negative, or zero during one precession period. However, the total work done by the spin Hall torque, $\oint dt(dE_s/dt)$, becomes zero in this case due to the symmetry of angular dependence of the spin Hall torque. This means that the spin Hall torque cannot compensate the damping torque, and thus, a steady precession assumed in the linearized LLG equation is not excited. This is evident in the numerically calculated magnetization trajectory shown in Fig. 5(b). For this case, the linearized LLG equation gives $|j_c| \rightarrow \infty$, indicating that the spin Hall torque cannot destabilize the magnetization. The same picture is also applicable, for example, in the absence of the applied field and $\beta = 0$.

However, an alternative mechanism can cause destabilization of the magnetization. As schematically shown in Figs. 6(a) and 6(c), there is a component of the damping like spin Hall torque that is orthogonal to the damping torque when $\Delta E_s = 0$. The spin Hall torque at this point

is parallel or antiparallel to the field torque depending on the position of the magnetization. When the spin Hall torque is sufficiently larger than the field torque, the magnetization moves from its equilibrium position even if the total energy supplied by the spin Hall torque is zero or negative. This leads to an instability that occurs before one precession finishes. In this case, it is expected that the critical current is damping-independent because the instability is induced as a competition between the spin Hall torque and the field torque, not the damping torque. The time evolution of the magnetization shown in Fig. 5 (b) represents such instability. The work reported in Refs.^{14,49} discusses a similar instability condition.

The above physical picture is also applicable in the presence of the fieldlike torque. The fieldlike torque, which acts like a torque due to the transverse field, modifies the equilibrium direction of the ferromagnet and thus the precession trajectory. Consequently, the amount of energy supplied by the spin Hall torque and the dissipation due to damping is changed when the fieldlike torque is present. Depending on the sign of β , the amount of the work done by the spin Hall torque increases or decreases compared to the case with $\beta = 0$. In our definition, positive β contributes to the increase of the supplied energy, resulting in the reduction of the critical current. The complex dependence of the critical current on α arises when the fieldlike torque is present.

To summarize the discussion, the critical current becomes damping dependent when the energy supplied by the spin Hall torque during a precession around the equilibrium is positive. The condition that meets this criteria depends on the relative direction of the spin Hall torque and the damping torque, as briefly discussed above. To derive an analytical formula that describes the condition at which the critical current becomes damping dependent is not an easy task except for some limited cases⁵³.

VI. CONCLUSION

In summary, we have studied the critical current needed to destabilize a perpendicularly magnetized ferromagnet by the spin Hall effect. The Landau-Lifshitz-Gilbert (LLG) equation that includes both the damping-like and fieldlike torques associated with the spin Hall effect is solved numerically and analytically. The critical current is found to have different dependence on the damping constant, i.e., the critical current scales with α^0 (damping-independent), α , and $\alpha^{1/2}$ depending on the sign of the fieldlike torque. The analytical formulas of the damping-dependent critical current, Eqs. (19), (20), and (21), are derived from the linearized LLG equation, which explain well the numerical results. We find that systems with fieldlike torque having the appropriate sign ($\beta > 0$ in our definition) are the most efficient way to reduce the critical current. For typical material parameters found in experiment, the critical current can be reduced to the order of 10^6 A/cm² when ferromagnets with rea-

sonable parameters are used.

ACKNOWLEDGMENTS

The authors acknowledge T. Yorozu, Y. Shiota, and H. Kubota in AIST for valuable discussion they had with us. This work was supported by JSPS KAKENHI Grant-in-Aid for Young Scientists (B), Grant No. 25790044, and MEXT R & D Next-Generation Information Technology.

Appendix A: Initial state of the numerical simulation

We assume that the magnetization in the absence of the applied field points to the positive z direction. In the presence of the field, the equilibrium direction moves from the z axis to the xy plane. Let us denote the zenith and azimuth angles of the initial state $\mathbf{m}(t=0)$ as θ and φ , i.e., $\mathbf{m}(t=0) = (\sin\theta \cos\varphi, \sin\theta \sin\varphi, \cos\theta)$. When the applied field points to the x -direction ($\mathbf{n}_H = \mathbf{e}_x$), the initial state is

$$\begin{pmatrix} \theta \\ \varphi \end{pmatrix}_{\mathbf{n}_H=\mathbf{e}_x} = \begin{pmatrix} \sin^{-1}[\sqrt{H_{\text{appl}}^2 + (\beta H_s)^2}/H_K] \\ \tan^{-1}(\beta H_s/H_{\text{appl}}) \end{pmatrix}, \quad (\text{A1})$$

where the value of φ is $0 < \varphi < \pi/2$ for $H_{\text{appl}} > 0$ and $\beta H_s > 0$, $\pi/2 < \varphi < \pi$ for $H_{\text{appl}} < 0$ and $\beta H_s > 0$, $\pi < \varphi < 3\pi/2$ for $H_{\text{appl}} < 0$ and $\beta H_s < 0$, and $3\pi/2 < \varphi < 2\pi$ for $H_{\text{appl}} > 0$ and $\beta H_s < 0$. On the other hand, when the applied field points to the y -direction ($\mathbf{n}_H = \mathbf{e}_y$), the initial state is

$$\begin{pmatrix} \theta \\ \varphi \end{pmatrix}_{\mathbf{n}_H=\mathbf{e}_y} = \begin{pmatrix} \sin^{-1}[(H_{\text{appl}} + \beta H_s)/H_K] \\ \pi/2 \end{pmatrix}, \quad (\text{A2})$$

where the range of the inverse sine function is $-\pi/2 \leq \sin^{-1}x \leq \pi/2$. We note that the choice of the initial state does not affect the evaluation of the critical current significantly, especially in the small field and current regimes.

Appendix B: Numerically evaluated critical current with different definition

As mentioned in Sec. III, the definition of the critical current has arbitrariness. As an example, we show the time evolution of m_z under the conditions of $\mathbf{n}_H = \mathbf{e}_x$, $H_{\text{appl}} = -30$ Oe, $\beta = 0$, and $j = 110 \times 10^6$ A/cm² in Fig. 7. In this case, the magnetization initially starts at $m_z = \cos[\sin^{-1}(H_{\text{appl}}/H_K)] \simeq 0.99$, and finally moves to a point $m_z \rightarrow 0.12$. Since the final state does not satisfy Eq. (9), this current, $j = 110 \times 10^6$ A/cm², should be regarded as the current smaller than the critical current in Sec. IV. However, from the analytical point of view, this current can be regarded as the current larger than

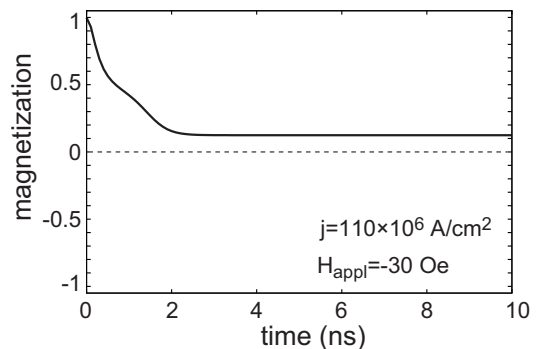


FIG. 7. Time evolution of the z component of the magnetization m_z in the presence of the longitudinal field with $H_{\text{appl}} = -30$ Oe, $\beta = 0$, and $j = 110 \times 10^6$ A/cm². The dotted line is a guide showing $m_z = 0$.

the critical current because the final state of the magnetization is far away from the initial equilibrium.

Regarding this point, we show the numerically evaluated critical current with a different definition. The magnetic state can be regarded as *unstable* when it finally arrives at a point far away from the initial state⁵⁴. Thus, for example, one can define the critical current as a minimum current satisfying

$$\lim_{t \rightarrow \infty} |m_z(t) - m_z(0)| > \delta, \quad (\text{B1})$$

where a small positive real number δ is chosen to be 0.1 here. Figure 8 summarizes the numerically evaluated critical current with the definition of Eq. (B1). The analytical formulas, Eqs. (19)-(21), still fit well with the numerical results. The absolute values of the damping-dependent critical current are slightly changed when the definition of the critical current is changed. This is because Eq. (B1) is more easily satisfied than Eq. (9), and thus the critical current in Fig. 8 is smaller than that shown in Fig. 4. However, the main results of this paper, such as the damping dependence of the critical current, are not changed by changing the definition of the critical current in the numerical simulations.

Appendix C: Energy change during a precession

As described in Sec. V, the linearized LLG equation assumes a steady precession of the magnetization due to the field torque when the current magnitude is close to the critical current. This is because the spin Hall torque compensates with the damping torque. Thus, Figs. 6(b) and 6(d) are obtained by substituting the solution of \mathbf{m} precessing a constant energy curve of \mathcal{E} into Eqs. (7) and (8).

When the transverse field is applied and $\beta = 0$, i.e., $\mathcal{E} = E$, where $E = -M \int d\mathbf{m} \cdot \mathbf{H}$, the precession trajectory on the constant energy curve of E is given by⁵⁵

$$m_x(E) = (r_2 - r_3)\text{sn}(u, k)\text{cn}(u, k), \quad (\text{C1})$$

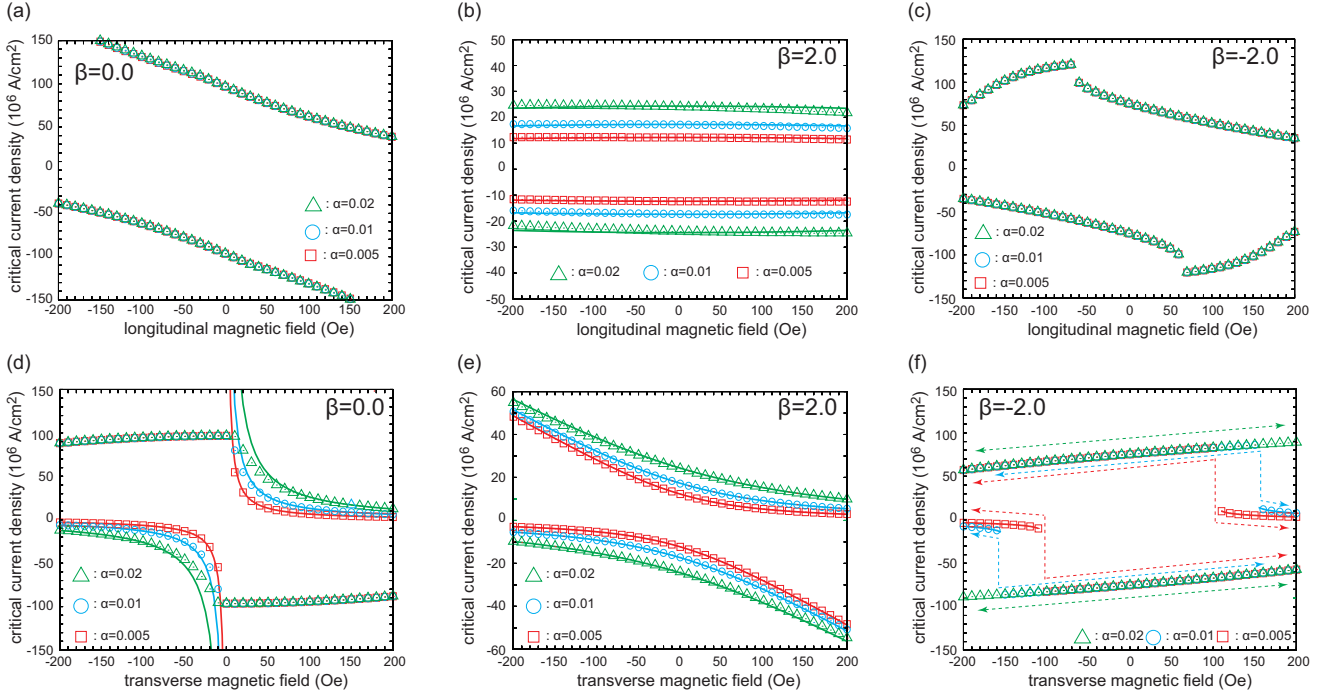


FIG. 8. Numerically evaluated critical currents with a different definition, Eq. (B1), in the presence of (a)-(c) the longitudinal ($\mathbf{n}_H = \mathbf{e}_x$) and (d)-(f) the transverse ($\mathbf{n}_H = \mathbf{e}_y$) fields, where the value of β is (a), (d) 0.0; (b), (e) 2.0; and (c), (f) -2.0 . The solid lines are the analytically estimated critical current described in Sec. V.

$$m_y(E) = r_3 + (r_2 - r_3)\text{sn}^2(u, k), \quad (\text{C2})$$

$$m_z(E) = \sqrt{1 - r_3^2 - (r_2^2 - r_3^2)\text{sn}^2(u, k)}, \quad (\text{C3})$$

where $u = \gamma\sqrt{H_t H_K/2}\sqrt{r_1 - r_3}t$, and r_ℓ are given by

$$r_1(E) = -\frac{E}{MH_{\text{appl}}}, \quad (\text{C4})$$

$$r_2(E) = \frac{H_{\text{appl}}}{H_K} + \sqrt{1 + \left(\frac{H_{\text{appl}}}{H_K}\right)^2 + \frac{2E}{MH_K}}, \quad (\text{C5})$$

$$r_3(E) = \frac{H_{\text{appl}}}{H_K} - \sqrt{1 + \left(\frac{H_{\text{appl}}}{H_K}\right)^2 + \frac{2E}{MH_K}}. \quad (\text{C6})$$

The modulus of Jacobi elliptic functions is $k = \sqrt{(r_2 - r_3)/(r_1 - r_3)}$. The precession period is

$$\tau(E) = \frac{2K(k)}{\gamma\sqrt{H_{\text{appl}}H_K/2}\sqrt{r_1 - r_3}}, \quad (\text{C7})$$

where $K(k)$ is the first kind of complete elliptic integral. The initial state is chosen to be $m_y(0) = r_3$. Figure 6(b) is obtained by substituting Eqs. (C1), (C2), and (C3) into Eqs. (7) and (8). We note that Eqs. (C1), (C2), and (C3) are functions of the energy density E . Since we are interested in the instability threshold near the equilibrium, the value of E is chosen close to the minimum energy E_{min} . In Fig. 6 (b), we use $E = E_{\text{min}} + (E_{\text{max}} - E_{\text{min}})/N$ with $N = 100$, where the minimum energy E_{min} and the maximum energy E_{max} are $E_{\text{min}} = -(MH_K/2)[1 + (H_{\text{appl}}/H_K)^2]$ and $E_{\text{max}} = -MH_{\text{appl}}$, respectively. The value of H_{appl} is chosen to be 50 Oe. Figure 6(d) is obtained in a similar way.

¹ M. I. Dyakonov and V. I. Perel, “Current-induced spin orientation of electrons in semiconductors,” *Phys. Lett. A* **35**, 459 (1971).
² J. E. Hirsch, “Spin Hall Effect,” *Phys. Rev. Lett.* **83**, 1834 (1999).
³ Y. K. Kato, R. C. Myers, A. C. Gossard, and D. D. Awschalom, “Observation of the Spin Hall Effect in Semiconductors,” *Science* **306**, 1910 (2004).

⁴ J. C. Slonczewski, “Current-driven excitation of magnetic multilayers,” *J. Magn. Magn. Mater.* **159**, L1 (1996).
⁵ L. Berger, “Emission of spin waves by a magnetic multilayer traversed by a current,” *Phys. Rev. B* **54**, 9353 (1996).
⁶ T. Yang, T. Kimura, and Y. Otani, “Giant spin-accumulation signal and pure spin-current-induced reversible magnetization switching,” *Nat. Phys.* **4**, 851

- (2008).
- ⁷ K. Ando, S. Takahashi, K. Harii, K. Sasage, J. Ieda, S. Maekawa, and E. Saitoh, “Electric Manipulation of Spin Relaxation Using the Spin Hall Effect,” *Phys. Rev. Lett.* **101**, 036601 (2008).
 - ⁸ L. Liu, C.-F. Pai, Y. Li, H. W. Tseng, D. C. Ralph, and R. A. Buhrman, “Spin-Torque Switching with the Giant Spin Hall Effect of Tantalum,” *Science* **336**, 555 (2012).
 - ⁹ L. Liu, C.-F. Pai, D. C. Ralph, and R. A. Buhrman, “Magnetization Oscillations Drive by the Spin Hall Effect in 3-Terminal Magnetic Tunnel Junctions Devices,” *Phys. Rev. Lett.* **109**, 186602 (2012).
 - ¹⁰ C.-F. Pai, L. Liu, Y. Li, H. W. Tseng, D. C. Ralph, and R. A. Buhrman, “Spin transfer torque devices utilizing the giant spin Hall effect of tungsten,” *Appl. Phys. Lett.* **101**, 122404 (2012).
 - ¹¹ M. Yamanouchi, L. Chen, J. Kim, M. Hayashi, H. Sato, S. Fukami, S. Ikeda, F. Matsukura, and H. Ohno, “Three terminal magnetic tunnel junction utilizing the spin Hall effect of iridium-doped copper,” *Appl. Phys. Lett.* **102**, 212408 (2013).
 - ¹² X. Fan, J. Wu, Y. Chen, M. J. Jerry, H. Zhang, and J. Q. Xiao, “Observation of the nonlocal spin-orbital effective field,” *Nat. Commun.* **4**, 1799 (2013).
 - ¹³ M. Cubukcu, O. Boule, M. Drouard, K. Garello, C. O. Avci, I. M. Miron, J. Langer, B. Ocker, P. Gambardella, and G. Gaudin, “Spin-orbit torque magnetization switching of a three-terminal perpendicular magnetic tunnel junction,” *Appl. Phys. Lett.* **104**, 042406 (2014).
 - ¹⁴ K.-S. Lee, S.-W. Lee, B.-C. Min, and K.-J. Lee, “Threshold current for switching of a perpendicular magnetic layer induced by spin Hall effect,” *Appl. Phys. Lett.* **102**, 112410 (2013).
 - ¹⁵ K.-S. Lee, S.-W. Lee, B.-C. Min, and K.-J. Lee, “Thermally activated switching of perpendicular magnet by spin-orbit spin torque,” *Appl. Phys. Lett.* **104**, 072413 (2014).
 - ¹⁶ J. Z. Sun, “Spin-current interaction with a monodomain magnetic body: A model study,” *Phys. Rev. B* **62**, 570 (2000).
 - ¹⁷ S. Ikeda, K. Miura, H. Yamamoto, K. Mizunuma, H. D. Gan, M. Endo, S. Kanai, J. Hayakawa, F. Matsukura, and H. Ohno, “A perpendicular-anisotropy CoFeB-MgO magnetic tunnel junction,” *Nat. Mater.* **9**, 721 (2010).
 - ¹⁸ S. Iihama, Q. Ma, T. Kubota, S. Mizukami, Y. Ando, and T. Miyazaki, “Damping of Magnetization Precession in Perpendicularly Magnetized CoFeB Alloy Thin Films,” *Appl. Phys. Express* **5**, 083001 (2012).
 - ¹⁹ S. Zhang, P. M. Levy, and A. Fert, “Mechanisms of Spin-Polarized Current-Driven Magnetization Switching,” *Phys. Rev. Lett.* **88**, 236601 (2002).
 - ²⁰ M. D. Stiles and A. Zangwill, “Anatomy of spin-transfer torque,” *Phys. Rev. B* **66**, 014407 (2002).
 - ²¹ M. Zwierzycki, Y. Tserkovnyak, P. J. Kelly, A. Brataas, and G. E. W. Bauer, “First-principles study of magnetization relaxation enhancement and spin transfer in thin magnetic films,” *Phys. Rev. B* **71**, 064420 (2005).
 - ²² A. Brataas, G. E. W. Bauer, and P. J. Kelly, “Non-collinear magnetoelectronics,” *Phys. Rep.* **427**, 157 (2006).
 - ²³ I. Theodonis, N. Kioussis, A. Kalitsov, M. Chshiev, and W. H. Butler, “Anomalous Bias Dependence of Spin Torque in Magnetic Tunnel Junctions,” *Phys. Rev. Lett.* **97**, 237205 (2006).
 - ²⁴ T. Taniguchi, S. Yakata, H. Imamura, and Y. Ando, “Determination of Penetration Depth of Transverse Spin Current in Ferromagnetic Metals by Spin Pumping,” *Appl. Phys. Express* **1**, 031302 (2008).
 - ²⁵ A. Ghosh, S. Auffret, U. Ebels, and W. E. Bailey, “Penetration Depth of Transverse Spin Current in Ultrathin Ferromagnets,” *Phys. Rev. Lett.* **109**, 127202 (2012).
 - ²⁶ A. A. Tulapurkar, Y. Suzuki, A. Fukushima, H. Kubota, H. Maehara, K. Tsunekawa, D. D. Djayaprawira, N. Watanabe, and S. Yuasa, “Spin-torque diode effect in magnetic tunnel junctions,” *Nature* **438**, 339 (2005).
 - ²⁷ H. Kubota, A. Fukushima, K. Yakushiji, T. Nagahama, S. Yuasa, K. Ando, H. Maehara, Y. Nagamine, K. Tsunekawa, D. D. Djayaprawira, N. Watanabe, and Y. Suzuki, “Quantitative measurement of voltage dependence of spin-transfer-torque in MgO-based magnetic tunnel junctions,” *Nat. Phys.* **4**, 37 (2008).
 - ²⁸ J. C. Sankey, Y.-T. Cui, J. Z. Sun, J. C. Slonczewski, R. A. Buhrman, and D. C. Ralph, “Measurement of the spin-transfer-torque vector in magnetic tunnel junctions,” *Nat. Phys.* **4**, 67 (2008).
 - ²⁹ S.-C. Oh, S.-Y. Park, A. Manchon, M. Chshiev, J.-H. Han, H.-W. Lee, J.-E. Lee, K.-T. Nam, Y. Jo, Y.-C. Kong, B. Dieny, and K.-J. Lee, “Bias-voltage dependence of perpendicular spin-transfer torque in asymmetric MgO-based magnetic tunnel junctions,” *Nat. Phys.* **5**, 898 (2009).
 - ³⁰ J. Grollier, V. Cros, H. Jaffrés, A. Hamzic, J. M. George, G. Faini, J. Ben Youssef, H. LeGall, and A. Fert, “Field dependence of magnetization reversal by spin transfer,” *Phys. Rev. B* **67**, 174402 (2003).
 - ³¹ H. Morise and S. Nakamura, “Stable magnetization states under a spin-polarized current and a magnetic field,” *Phys. Rev. B* **71**, 014439 (2005).
 - ³² D. Gusakova, D. Houssameddine, U. Ebels, B. Dieny, L. Buda-Prejbeanu, M. C. Cyrille, and B. Delaët, “Spin-polarized current-induced excitations in a coupled magnetic layer system,” *Phys. Rev. B* **79**, 104406 (2009).
 - ³³ T. Taniguchi, S. Tsunegi, H. Kubota, and H. Imamura, “Self-oscillation in spin torque oscillator stabilized by field-like torque,” *Appl. Phys. Lett.* **104**, 152411 (2014).
 - ³⁴ T. Taniguchi, S. Tsunegi, H. Kubota, and H. Imamura, “Large amplitude oscillation of magnetization in spin-torque oscillator stabilized by field-like torque,” *J. Appl. Phys.* **117**, 17C504 (2015).
 - ³⁵ J. Kim, J. Sinha, M. Hayashi, M. Yamanouchi, S. Fukami, T. Suzuki, S. Mitani, and H. Ohno, “Layer thickness dependence of the current-induced effective field vector in Ta|CoFeB|MgO,” *Nat. Mater.* **12**, 240 (2013).
 - ³⁶ K. Garello, I. M. Miron, C. O. Avci, F. Freimuth, Y. Mokrousov, S. Blügel, S. Auffret, O. Boule, G. Gaudin, and P. Gambardella, “Symmetry and magnitude of spin-orbit torques in ferromagnetic heterostructures,” *Nat. Nanotech.* **8**, 587 (2013).
 - ³⁷ X. Qiu, P. Deorani, K. Narayanapillai, K.-S. Lee, K.-J. Lee, H.-W. Lee, and H. Yang, “Angular and temperature dependence of current induced spin-orbit effective fields in Ta/CoFeB/MgO nanowires,” *Sci. Rep.* **4**, 4491 (2014).
 - ³⁸ C.-F. Pai, M.-H. Nguyen, C. Belvin, L. H. Vielal-Leao, D. C. Ralph, and R. A. Buhrman, “Enhancement of perpendicular magnetic anisotropy and transmission of spin-Hall-effect-induced spin currents by a Hf spacer layer in W/Hf/CoFeB/MgO layer structures,” *Appl. Phys. Lett.* **104**, 082407 (2014).
 - ³⁹ J. Kim, J. Sinha, S. Mitani, M. Hayashi, S. Takahashi, S. Maekawa, M. Yamanouchi, and H. Ohno, “Anomalous temperature dependence of current-induced torques

- in CoFeB/MgO heterostructures with Ta-based underlayers,” *Phys. Rev. B* **89**, 174424 (2014).
- ⁴⁰ J. Torrejon, J. Kim, J. Sinha, S. Mitani, M. Hayashi, M. Yamanouchi, and H. Ohno, “Interface control of the magnetic chirality in CoFeB/MgO heterostructures with heavy-metal underlayers,” *Nat. Commun.* **5**, 4655 (2014).
- ⁴¹ I. M. Miron, K. Garello, G. Gaudin, P.-J. Zermatten, M. V. Costache, S. Auffret, S. Bandiera, B. Rodmacq, A. Schuhl, and P. Gambardella, “Perpendicular switching of a single ferromagnetic layer induced by in-plane current injection,” *Nature* **476**, 189 (2011).
- ⁴² K.-W. Kim, S.-M. Seo, J. Ryu, K.-J. Lee, and H.-W. Lee, “Magnetization dynamics induced by in-plane currents in ultrathin magnetic nanostructures with Rashba spin-orbit coupling,” *Phys. Rev. B* **85**, 180404 (2012).
- ⁴³ P. M. Haney, H.-W. Lee, K.-J. Lee, A. Manchon, and M. D. Stiles, “Current induced torques and interfacial spin-orbit coupling: Semiclassical modeling,” *Phys. Rev. B* **87**, 174411 (2013).
- ⁴⁴ P. M. Haney, H.-W. Lee, K.-J. Lee, A. Manchon, and M. D. Stiles, “Current-induced torques and interfacial spin-orbit coupling,” *Phys. Rev. B* **88**, 214417 (2013).
- ⁴⁵ M. Jamali, K. Narayanapillai, X. Qiu, L. M. Loong, A. Manchon, and H. Yang, “Spin-Orbit Torques in Co/Pd Multilayer Nanowires,” *Phys. Rev. Lett.* **111**, 246602 (2013).
- ⁴⁶ G. Yu, P. Upadhyaya, Y. Fan, J.G. Alzate, W. Jiang, K. L. Wong, S. Takei, S. A. Bender, L.-T. Chang, Y. Jiang, M. Lang, J. Tang, Y. Wang, Y. Tserkovnyak, P. K. Amiri, and K. L. Wang, “Switching of perpendicular magnetization by spin-orbit torques in the absence of external magnetic fields,” *Nat. Nanotech.* **9**, 548 (2014).
- ⁴⁷ C. O. Pauyac, X. Wang, M. Chshiev, and A. Manchon, “Angular dependence and symmetry of Rashba spin torque in ferromagnetic structures,” *Appl. Phys. Lett.* **102**, 252403 (2013).
- ⁴⁸ J. Torrejon, F. Garcia-Sanchez, T. Taniguchi, J. Shinha, S. Mitani, J.-V. Kim, and M. Hayashi, “Current-driven asymmetric magnetization switching in perpendicularly magnetized CoFeB/MgO heterostructures,” *Phys. Rev. B* **91**, 214434 (2015).
- ⁴⁹ L. Liu, O. J. Lee, T. J. Gudmundsen, D. C. Ralph, and R. A. Buhrman, “Current-Induced Switching of Perpendicularly Magnetized Magnetic Layers Using Spin Torque from the Spin Hall Effect,” *Phys. Rev. Lett.* **109**, 096602 (2012).
- ⁵⁰ L. You, O. Lee, D. Bhowmik, D. Labanowski, J. Hong, J. Bokor, and S. Salahuddin, arXiv:1409.0620.
- ⁵¹ (), a similar approach was recently developed by Yan and Bazaliy, *Phys. Rev. B* **91** 214424 (2015).
- ⁵² (), the analytical formula of the critical current corresponding the case of $\beta = 0$ is discussed in Ref.¹⁴. The formula of Ref.¹⁴ is applicable to a large damping limit ($\alpha > 0.03$), while we are interested in a low damping limit.
- ⁵³ G. Bertotti, I. Mayergoyz, and C. Serpico, *Nonlinear magnetization Dynamics in Nanosystems* (Elsevier, Oxford, 2009).
- ⁵⁴ S. Wiggins, “Introduction to applied nonlinear dynamical systems and chaos,” (Springer, 2003) Chap. 1.
- ⁵⁵ T. Taniguchi, “Nonlinear analysis of magnetization dynamics excited by spin Hall effect,” *Phys. Rev. B* **91**, 104406 (2015).